

Homeostatic Criticality in Neuronal Networks

Gustavo Menesse,¹ Bóris Marin,² Mauricio Girardi-Schappo,³ and Osame Kinouchi^{1,*}

¹*Departamento de Física, FFCLRP, Universidade de São Paulo,*

Ribeirão Preto, SP, 14040-901, Brazil

²*Centro de Matemática Computação e Cognição,*

Universidade Federal do ABC, São Bernardo do Campo, SP, 09606-070, Brazil

³*Department of Physics, University of Ottawa, Ottawa, ON, K1N 6N5, Canada*

In self-organized criticality (SOC) models, as well as in standard phase transitions, criticality is only present for vanishing driving external fields $h \rightarrow 0$. Considering that this is rarely the case for natural systems, such a restriction poses a challenge to the explanatory power of these models. Besides that, in models of dissipative systems like earthquakes, forest fires, and neuronal networks, there is no true critical behavior, as expressed in clean power laws obeying finite-size scaling, but a scenario called “dirty” criticality or self-organized quasi-criticality (SOqC). Here, we propose simple homeostatic mechanisms which promote self-organization of coupling strengths, gains, and firing thresholds in neuronal networks. We show that with adequate timescale separation between coupling strength and firing thresholds dynamics, near criticality (SOqC) can be reached and sustained even in the presence of external inputs. The firing thresholds adapt to and cancel the inputs (h decreases towards zero), a phenomenon similar to perfect adaptation in sensory systems. Similar mechanisms can be proposed for the couplings and local thresholds in spin systems and cellular automata, which could lead to applications in earthquake, forest fire, stellar flare, voting, and epidemic modeling.

The idea of self-organized criticality (SOC) [1], in which a system would have a critical point as an attractor in the absence of any fine-tuning of parameters, in some sense has never truly been achieved. The most successful models in this ideal are usually conservative, such as Abelian sandpiles [2–4], but conservation can be thought as a form of fine-tuning, that is, the dissipation parameter in the transmission of grains must be zero. Also, the infinite

* okinouchi@gmail.com; Corresponding author

separation of time scales between driving and avalanches in SOC models can be viewed as yet another fine-tuning requirement.

When we consider dissipative systems such as earthquakes, forest fires or neural networks, we find that only self-organized quasicriticality (SOqC), where the system performs stochastic oscillations around the critical point, holds [5, 6]. Several of such models include continuous drive and dissipation that can be viewed as homeostatic mechanisms which tune the network toward the critical region.

In the case of neuronal networks, the experimental motivation for SOqC models is to explain neuronal avalanches [7–11]. The main studied homeostatic mechanisms are related to synaptic dynamics [12–14] but dynamical gains [15–18] and firing thresholds have also been considered [26] (for a review see [20]).

In the absence of homeostatic mechanisms, a critical regime is obtained only with strong and non-local fine-tuning on, for example, all coupling weights (synapses) W_{ij} , so that the distribution $P(W_{ij})$ must have average $\langle W_{ij} \rangle = W = W_c$ (the control parameter). With homeostasis, this constraint is relaxed: now we can start from any distribution $P_{t=0}(W_{ij})$ and, after a transient (the self-organization process), one obtains a stationary $P^*(W_{ij}) \equiv \lim_{t \rightarrow \infty} P(W_{ij})$ where $W^* \equiv \lim_{t \rightarrow \infty} \langle W_{ij} \rangle \approx W_c$. Similar reasoning applies to neuronal gains (Γ_i) and firing thresholds (θ_i).

One important aspect in any SOC model is that phase transitions, and therefore criticality, exist only for zero or very small external field [21], so any homeostatic mechanism will need to self-organize the system to a state where the effective external field vanishes.

Here, first we show how such a homeostatic mechanism works in a simple analytic mean-field model. Then, we present simulation results for sparse random networks with K neighbors per node. The mechanisms are simple and very general: they can be adapted to systems composed of other units like spins, cellular automata, discrete time maps and continuous time neurons with pulse coupling given by weights W_{ij} .

We consider a network of N discrete-time stochastic leaky integrate-and-fire neurons [15, 16, 18, 22–25]. A Boolean indicator $X_i \in \{0, 1\}$, $i = 1, \dots, N$, denotes silence ($X_i = 0$) or the firing of an action potential (spike, $X_i = 1$). The membrane potential of neuron i evolves according to:

$$V_i(t+1) = \mu_i V_i(t) + I_i + \frac{1}{K} \sum_{j=1}^K W_{ij} X_j(t), \quad (1)$$

where $0 \leq \mu_i \leq 1$ are leakage parameters and I_i are external inputs. The directed synaptic weight matrix W_{ij} has exactly K incoming links from j to i . The outgoing links, by this construction, have a binomial distribution with average K and standard deviation $\sigma = \sqrt{K(1 - K/(N - 1))}$.

If at time step t the neuron fires, its membrane potential is reset, $V_i(t+1) = 0$. Otherwise, the neuron follows Eq. (1). A spike occurs with probability:

$$P(X_i(t) = 1 | V_i(t)) \equiv \Phi_i(V_i(t)) , \quad (2)$$

where $\Phi(V)$ is the so-called firing function. The model incorporates an absolute refractory period of one time step by imposing $\Phi(0) = 0$.

For this class of models, there are no strong requirements on the firing function Φ besides sigmoid shape, but for analytical convenience we use the so called linear-saturating function [15, 19, 24]:

$$\Phi_i(V_i) = \begin{cases} 0 & \text{if } V_i < \theta_i \\ \Gamma_i (V_i - \theta_i) & \text{if } 0 < V_i < V_i^S \\ 1 & \text{if } V_i > V_i^S \end{cases} \quad (3)$$

where $V_i^S = 1/\Gamma_i + \theta_i$ is the saturation potential. Here, θ_i represents the firing threshold for neuron i .

In the absence of homeostatic tuning (which we call the static model), assuming that the distribution $P(W_{ij})$ has finite variance, the average synaptic weight $W = \langle W_{ij} \rangle$ can be taken as a control parameter. The same applies to the neuronal gains Γ_i , firing thresholds θ_i , leakage parameters μ_i and inputs I_i , so that $\Gamma = \langle \Gamma_i \rangle$ and $\mu = \langle \mu_i \rangle$ can also be considered as control parameters. Interpreting $\theta = \langle \theta_i \rangle$ as the average local field (local adaptation current) and $I = \langle I_i \rangle$ as the average external field (external input current), we have that $h = I - \theta$ is the total or effective field.

The fraction of spiking neurons, or firing density, $\rho(t) = \langle X_i(t) \rangle \equiv \frac{1}{N} \sum_{i=1}^N X_i(t)$ represents the activity of the system. Its time average $\langle \rho(t) \rangle_t$, calculated after disregarding transients, is taken as the relevant order parameter.

When Γ, W and θ are fixed (static model), a mean-field approximation (equivalent to taking the $K \rightarrow \infty$ limit) can be calculated from:

$$\rho(t+1) = \int \Phi(V) P(V, t) dV , \quad (4)$$

where $P(V, t)$ is the distribution of voltages at time t [15, 18].

For $\mu = 0$, considering the case where the stationary potentials fall within the linear ($0 < V_i < V_i^S$) branch of equation (3), the solution leads to the mean-field map:

$$\rho(t+1) = (1 - \rho(t))\Gamma(W\rho(t) + h) , \quad (5)$$

The stationary state is obtained solving Eq. (5):

$$\rho^\pm = \frac{\Gamma W - 1 - \Gamma h \pm \sqrt{(\Gamma W - 1 - \Gamma h)^2 + 4\Gamma^2 W h}}{2\Gamma W} . \quad (6)$$

When the field is $h < 0$, we have a discontinuous (first order) phase transition and, when $h > 0$, there is always activity $\rho > 0$ and no transition [15, 19].

For $h = 0$, we have a second order phase transition, which is given by:

$$\rho(W, \Gamma) \sim \left(\frac{W - W_c(\Gamma)}{W_c(\Gamma)} \right)^\beta , \quad (7)$$

for $W > W_c = 1/\Gamma$ and $\rho = 0$ (absorbing state) for $W < W_c$. The order parameter exponent is $\beta = 1$. The hyperbola $W_c(\Gamma) = 1/\Gamma$ is a critical line in the $W \times \Gamma$ plane. Similarly to what occurs in the Ising model, where the important variable is the combined quantity J/T , here, the important variable is $\tilde{W} \equiv \Gamma W$, which defines the critical point $\tilde{W}_c = 1$ (see Fig. 1). For $\tilde{W} \geq 2$ we see a period-2 orbit in the activity $\rho(t)$, which is not relevant to the present discussion and has been studied in detail elsewhere [15, 19].

For random networks, a continuous phase transition is also observed:

$$\rho(\tilde{W}; \mu) = C(K, \mu) \left(\frac{\tilde{W} - \tilde{W}_c(\mu)}{\tilde{W}} \right) , \quad (8)$$

(see Fig. 1). The critical point is independent of K , but shows a dependence on μ that seems to follow $\tilde{W}_c(\mu) = (1 - \mu)\tilde{W}_c(0)$ (see [26] for the infinite K limit). Meanwhile, $\beta = 1$ is independent of K and μ , which is compatible with the finding of mean-field DP exponents in a large set of experiments, for networks with presumable very different wiring topology and leakage parameters [7, 11, 27].

Notice that, for zero activity, Eq. (1) has a steady state $V^* = I/(1 - \mu)$. From the condition $V^* > \theta$ for firing, we define the effective field $h = I - (1 - \mu)\theta$ for general μ . At the transition to the active phase, $V^* = \theta$, so that h must be zero [19].

To tune the network to the critical region [5, 12, 13, 15, 16, 18–20]) we introduce our model with homeostatic mechanisms. The calculations are done at the mean-field level

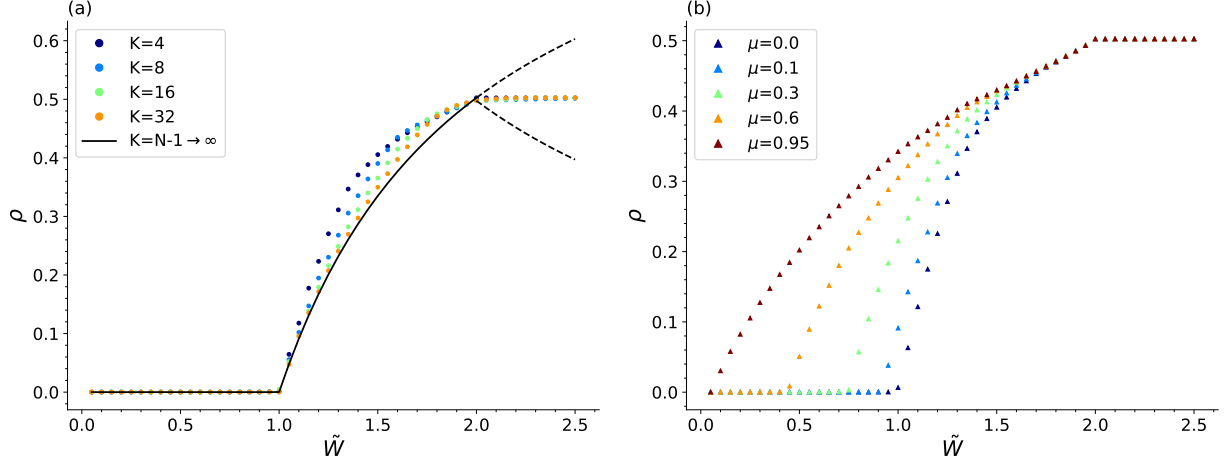


FIG. 1. a) Order parameter $\rho(\tilde{W}; \mu = 0)$ as a function of \tilde{W} for different number of neighbors K . From left to right, $K = 4, 8, 16, 32$ and mean-field (solid); b) $\rho(\tilde{W}; K = 4)$ for varying leakage parameter μ . From right to left, $\mu = 0, 0.1, 0.3, 0.6$ and 0.95 . Networks size $N = 10,000$. The bifurcation at $\tilde{W} = 2$ leads to the creation of a period-2 synchronous regular state [15, 19].

for $\mu = 0$, but similar results can be shown in simulations for general K and μ . First, we apply a depressing-recovering dynamic to the control parameter $\tilde{W}(t) \equiv \langle \Gamma_i W_{ij}(t) \rangle$. Following biological motivations, we propose two mechanisms: one for neuronal gains $\Gamma_i(t)$ and another for synaptic weights $W_{ij}(t)$. We use dynamics similar to the Levina-Hermann-Geisel synaptic dynamics [12] for both variables:

$$W_{ij}(t+1) = W_{ij}(t) + \frac{1}{\tau_W} \left(\frac{A_i(1-\mu_i)}{\Gamma_i(t)} - W_{ij}(t) \right) - U_W W_{ij}(t) X_j(t), \quad (9)$$

$$\Gamma_i(t+1) = \Gamma_i(t) + \frac{1}{\tau_\Gamma} (B_i - \Gamma_i(t)) - U_\Gamma \Gamma_i(t) X_i(t). \quad (10)$$

The dynamics for synaptic weights (W_{ij}) has a basal level $A_i(1-\mu_i)/\Gamma_i(t)$, a recovery time τ_W and a depressing factor $0 < U_W < 1$ related to the fraction of neurotransmitter vesicles depleted in the synapse due to a presynaptic spike $X_j = 1$. A similar idea applies to the dynamics of membrane excitability (neuronal gains Γ_i).

The coupling between $W_{ij}(t)$ and Γ_i is necessary to get $W^* = (1-\mu)/\Gamma^*$, resulting in $\tilde{W}_c = 1-\mu$. This is a small non-locality in the basal level of synaptic weights, which says that the effective recovery time of synapses τ_W depends on the neuronal gain Γ_i and on the leakage parameter μ_i . In biological neurons, this coupling between synapses and neuronal excitability could be mediated by retrograde signals (active dendritic spikes [28, 29]). Specifically, it is known that excitability of the cell body down regulates neurotransmitter re-uptake by using

endocannabinoids produced pre-synaptically [30, 31].

Notice that in the $\Gamma_i(t)$ dynamics, the activity signal X_i is local, referring to the cell body with gain Γ_i . Averaging over sites (in the $\mu = 0$ case), the MF equations become:

$$W(t+1) = W(t) + \frac{1}{\tau_W} \left(\frac{A}{\Gamma} - W(t) \right) - U_W W(t) \rho(t), \quad (11)$$

$$\Gamma(t+1) = \Gamma(t) + \frac{1}{\tau_\Gamma} (B - \Gamma(t)) - U_\Gamma \Gamma(t) \rho(t). \quad (12)$$

To achieve criticality, we also need h to be 0. For spin systems, zero external magnetic field is a natural condition, despite being a fine-tuning operation seldom discussed in the literature of neuronal avalanches [19, 21]. Here, for integrate-and-fire neurons, this condition is not so natural: we must fine-tune $\theta_c = I/(1 - \mu)$ in order to achieve $h_c = 0$. Therefore, we also need a homeostatic mechanism to set h to zero.

We propose a simple firing-threshold adaptation mechanism:

$$\theta_i(t+1) = \theta_i(t) - \frac{1}{a\tau_W} \theta_i(t) + bU_W \theta_i(t) X_i(t), \quad (13)$$

$$\theta(t+1) = \theta(t) - \frac{1}{a\tau_W} \theta(t) + bU_W \theta(t) \rho(t), \quad (14)$$

where $\theta(t) \equiv \langle \theta_i(t) \rangle$. Here, the θ timescale is presented as a fraction a, b of the timescales for synaptic dynamics (U_W, τ_W).

From the mean fields equations (5), (11), (12) and (14), we get the following relevant fixed point:

$$\rho^* = \frac{1}{ab \tau_W U_W}, \quad (15)$$

$$\Gamma^* = \frac{B}{1 + \frac{\tau_\Gamma U_\Gamma}{ab \tau_W U_W}}, \quad (16)$$

$$W^* = \frac{A}{\Gamma^* (1 + \frac{1}{ab})}, \quad (17)$$

$$h^* = I - \theta^* = \rho^* \left(W^* - \frac{1}{\Gamma^*} \right) + \frac{\rho^{*2}}{\Gamma^*} - \mathcal{O}(\rho^3) \quad (18)$$

Comparing the critical point ($\rho_c = 0^+, \tilde{W}_c = W\Gamma = 1, h_c = 0$) to the fixed point above, we can see that two conditions are needed to reach quasi-criticality. First, we need $ab \gg 1$ (large separation of W and θ time scales), which is a very common feature in SOC models [32]. Second, we need to fine-tune $A = \langle A_i \rangle \approx 1$ to have $h = \mathcal{O}(\rho^{*2}) \approx 0$ [26].

We use \tilde{W} time scales in the order of 100 ms ($\tau_W = 300$ and $\tau_\Gamma = 100$). Therefore, \tilde{W} evolves at timescales comparable to that of network activity propagation. On the other

hand, we model the adaptive threshold mechanism as a long-term homeostatic regulation ($a > 10^3$), which means that this adaptation process occurs on a timescale slower than that of network dynamics.

The \tilde{W}^* component of the fixed point is always subcritical, but tends to the critical value when $(ab) \rightarrow \infty$. From a biological perspective, staying in the vicinity of a subcritical state might be advantageous, as it would decrease the risk of spontaneous runaway activity linked to dysfunctional regimes such as epilepsy [33].

For a robust quasi critical regime, as reflected in near critical avalanches, the system needs to evolve towards a stable fixed point not far from the true critical point, as quickly as possible, while keeping oscillations around the equilibrium to a minimum. This can be achieved by minimizing the spectral radius of the Jacobian matrix. In Fig. 2(top), we study the stability of fixed point $(\rho^*, \Gamma^*, W^*, \theta^*)$ with respect to timescale separation parameters a, b when $A=1$. Colored regions indicate dynamics with stable fixed points.

Parameters region with leading eigenvalue modulus $|\lambda_D| < 0.9999$ and argument $\omega < 0.01$ give rise to dynamics with $|h| < 10^{-4}$, see simulation results in 2(bottom). Thus, for a given value for parameter a , there is a range of b values (coarse tuning) that allow the homeostatic mechanism to reach and maintain h and \tilde{W} values low enough ($|h| \approx \mathcal{O}(10^{-4})$ [21] and $\tilde{W} \approx \tilde{W}_c - \mathcal{O}(10^{-2})$) to produce critical avalanches and quasi-critical behavior.

Results for mean field and random network simulations are shown in Fig.3a. Initial conditions were chosen from different distributions (constant values for $\Gamma_i(0) = [0.5, 1.5]$, normal distribution $\mathcal{N}_{[0.75, 0.01]}$ and $\mathcal{N}_{[1.25, 0.01]}$ for $\theta_i(0)$, and uniform distribution $\mathcal{U}_{[0, 2]}$ for $W_{ij}(0)$). In all cases, trajectories in $\tilde{W} \times h$ space (see Fig4) show low amplitude stochastic oscillations around a slightly subcritical point, with mean amplitude ≈ 0.01 in \tilde{W} and 10^{-4} in h . In Fig3b, we depict the activity $\rho(t)$, which displays SOqC avalanches with a power law regime sufficient to explain experimental data.

We measured the size and duration of avalanches for trajectories with 10^6 time steps. Near the critical point, we expect avalanche sizes S and durations D to be distributed according to $F(s) = P(S > s) \propto s^{1-\tau}$ and $F(d) = P(D > d) \approx d^{1-\tau_d}$ respectively, with exponents $\tau = 3/2$ and $\tau_d = 2$ (mean-field Directed Percolation class [15]).

The emergence of avalanches, even with the correct exponents, is not a sufficient condition for identifying criticality [34], therefore we investigate the relationship between mean avalanche size and duration $\langle s \rangle (d)$ leading to the exponent relation $m = (\tau_D - 1)/(\tau_S - 1)$.

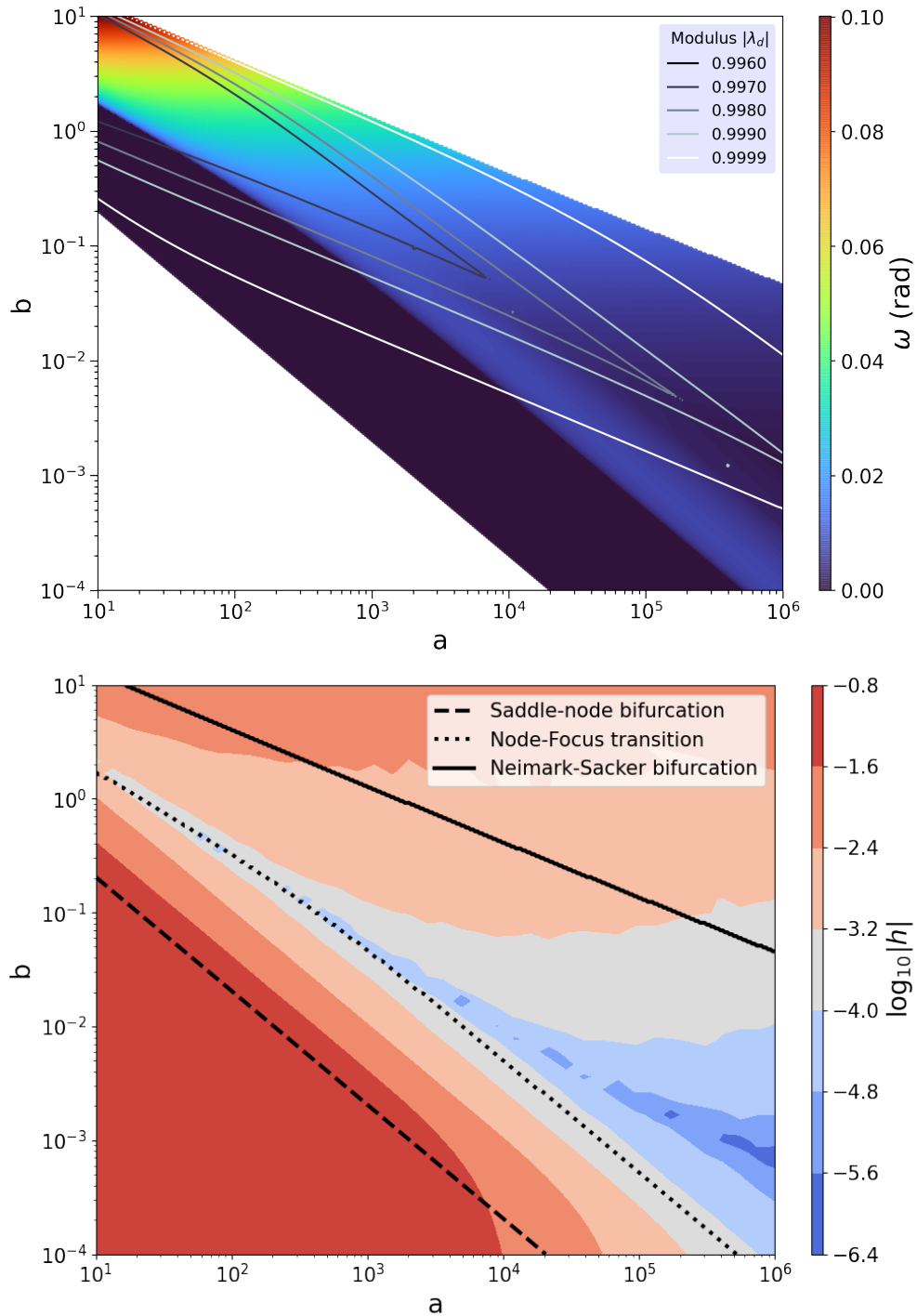


FIG. 2. Mean-field stability diagram. (top) Argument (heat-map) and modulus (contour lines) of leading eigenvalue. Colored regions correspond to systems with a stable fixed point, and white regions to dynamics with unstable fixed points. (bottom) Effective field $|h|$ in logarithmic scale obtained in random network simulations. Limited power law avalanches, sufficient to explain experiments, are observed in the blue region. Bifurcation and transition lines also shown.

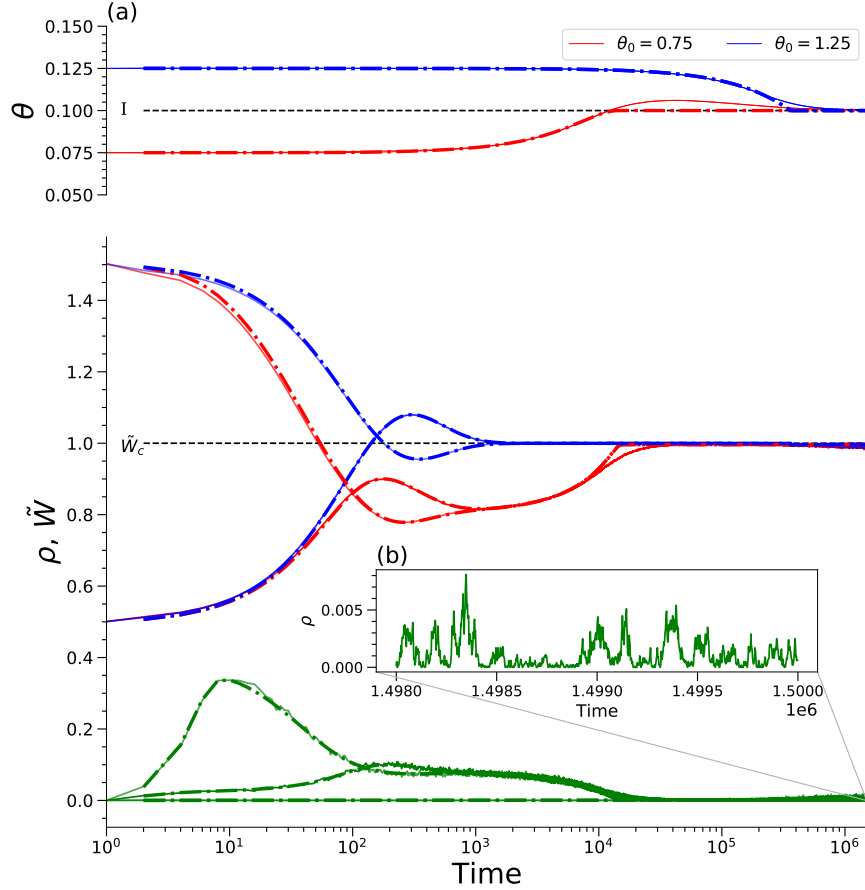


FIG. 3. Self-organization of $\tilde{W}(t)$ and $\theta(t)$ from different initial conditions (blue and red). The target values are $\theta_c = I = 0.1$ (or $h = I - \theta = 0$) and $\tilde{W}_c = 1$. (a) Time series for $\theta(t)$, $\tilde{W}(t)$ and $\rho(t)$ (green). Mean field (dashed lines) and random network (solid lines) with $K = 32$ and $N=10000$. (b) Avalanche behavior for stationary $\rho(t)$. Parameters: $\tau_W = 300, \tau_\Gamma = 100, U_W = 0.01, U_\Gamma = 0.01, B = 1, A = 1, a=5000$ and $b=0.05$.

At criticality, we expect $m = 2$. To compare simulation results with theory, we use the distance to criticality coefficient $dcc = m - m_{fitted}$, as proposed in [35]. In this case, to compute dcc , we take the mean value of m fitted for the simulations with different N for three a, b values.

Fig. 5 show how the finite-size scaling of avalanche sizes and durations improves with increasing timescale separation a . However, perfect finite-size scaling is never achieved for finite a values. Since SOqC criticality is not perfect [6], our results are in good agreement with what is expected when the underlying phase transition is on the DP class. Fig. 6 shows that the exponent's relation also tends to agree with theory for increasing separation of time scales $a \rightarrow \infty$, resulting in small distance to criticality ($dcc < 0.01$) for $a = 10^6$.

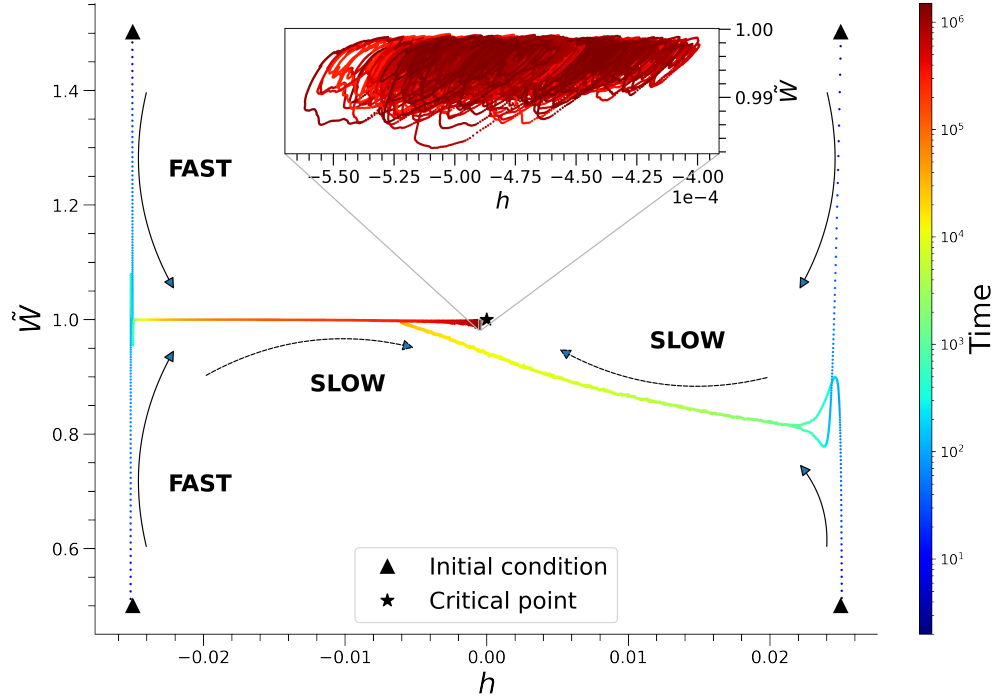


FIG. 4. Phase space. Self-organization of \tilde{W} and h for four different initial conditions and input $I=0.1$, simulated in a random network with $K = 32$ and $N=10000$. Initial conditions average value are combination of $\theta = [0.75, 1.25]$ and $\Gamma = [0.5, 1.5]$ with $W = 1$. Parameters:

$$\tau_W = 300, \tau_\Gamma = 100, U_W = 0.01, U_\Gamma = 0.01, a=5000 \text{ and } b=0.05$$

Our neuronal network model self-organizes toward quasi-criticality even in the presence of nonzero inputs I_i . This is an important result, because real neurons always receive external inputs from other areas. The homeostatic thresholds θ_i produce $|h| < 10^{-4}$, an (almost exact) adaptation to the inputs. That is, instead of to fine-tune $h = 0$, as done in standard phase transitions and previous SOC/SOqC models, here we self-organize the local fields $h_i(t) = I_i - \theta_i(t)$ toward zero. This is not a mere detail, but a crucial ingredient for a truly self-organized critical model.

The self-organized system hovers around a stable (quasi critical) fixed point with small amplitude orbits, minimizing the large stochastic oscillations observed in previous models [16, 18, 19]. In particular, the system gets closer to criticality as the timescale ratio $a = \tau_\theta/\tau_W = \tau_\theta/\tau_\Gamma$ increases.

Regarding the unavoidable fine-tuning $A \approx 1$ emerging from our analysis, we need to remember Hernandez-Urbina and Herrmann: fine-tuning a hyperparameter in local homeostatic mechanisms is very different from global fine-tuning in the original static model control

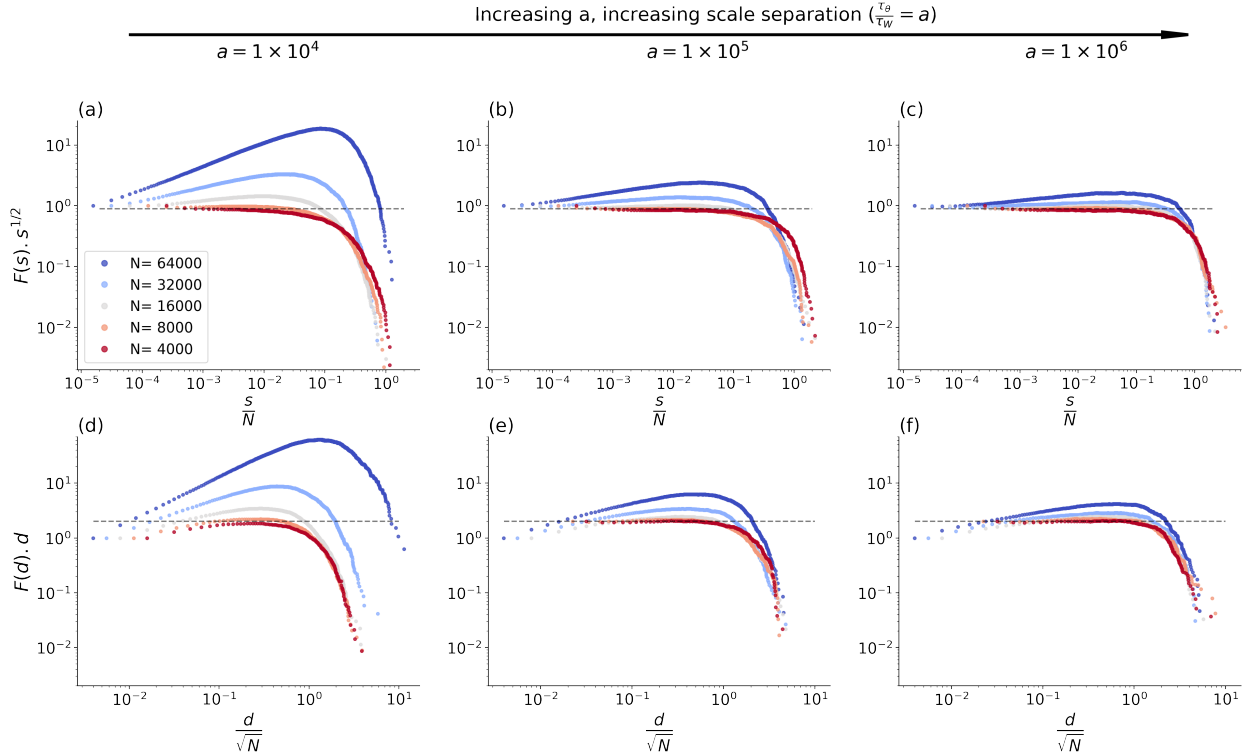


FIG. 5. Finite-size scaling of avalanche size and duration for increasing values of a

and network size N . First row shows scaling for sizes, and second row for durations. The scaling improves with increasing a , reaching good finite-size scaling when $a \rightarrow \infty$. Results obtained for a quenched simulation of a directed random network with $K = 32$. Parameters: (a,d) $a = 10^4$ and $b = 8 \times 10^{-2}$, (b,e) $a = 10^5$ and $b = 10^{-2}$ and (c,f) $a = 10^6$ and $b = 10^{-3}$.

parameters $\{W_{ij}, h_i\}$ [20, 36]. Anyway, a challenge to the community persists: could we get $A \approx 1$ without any form of fine-tuning? We conjecture that this is impossible: the need for $h^* \approx 0$ will impose strict conditions similar to $A \approx 1$ to any other homeostatic model [26].

Generalizing our results, it is plausible that any system under the influence of external fields like I (say, a magnetic field H in spin systems) — as in earthquakes, forest fires, voting or epidemics models based in spins, cellular automata or even continuous time integrate-and-fire dynamics — can achieve a near critical regime through the inclusion of adaptive opposite local fields (as $-\theta_i(t)$ here) whose timescale should be much slower than that of the rest of the system.

Nonetheless, it is not clear how time-varying inputs $I_i(t)$ would affect the behavior of our system. We conjecture that the thresholds $\theta_i(t)$ would produce a phenomenon akin to sensory adaptation [37, 38]. If so, for short time scales, our homeostatic networks would respond

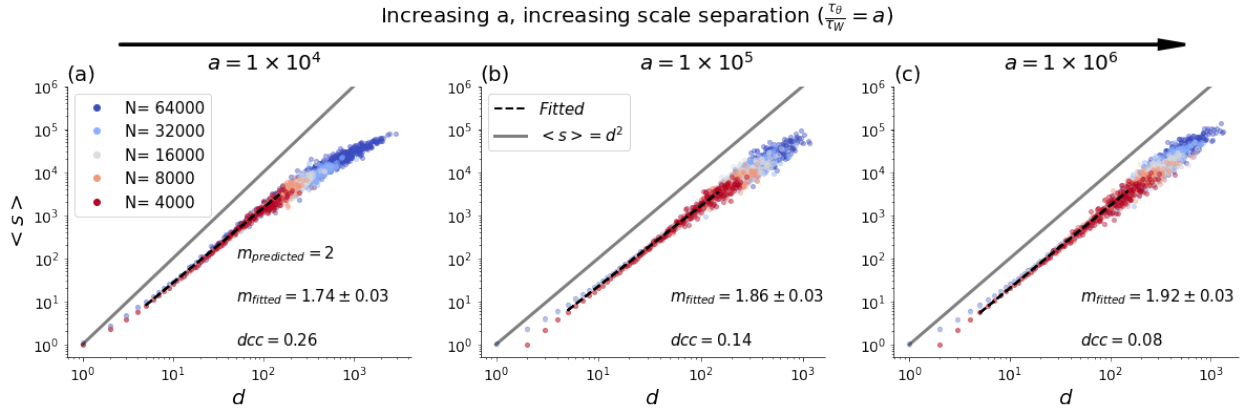


FIG. 6. Average avalanche size vs duration for increasing values of timescale separation a and network size N . Directed random network with $K = 32$. Average initial conditions: $\theta(0) = 0.09$, $\Gamma(0) = 0.75$ with $W(0) = 1$, input $I = 0.1$. (a) Parameters $a = 10^4$ and $b = 8 \times 10^{-2}$; (b) $a = 10^5$ and $b = 10^{-2}$ and (c) $a = 10^6$ and $b = 10^{-3}$. Fitted exponent relation (m_{fitted}) and distance to criticality coefficient (dcc) also shown.

to the derivatives of the external signal, as opposed to signal intensity, which could lead to novel computational properties. This means that the results of Kinouchi and Copelli [39] on optimization of dynamic range in critical networks would be challenged, or better, need to consider sensory systems with adaptation. This important issue will be studied in a future extended paper.

ACKNOWLEDGMENTS

GM would like to thank CAPES for financial support. OK acknowledges CNAIPS-USP and CNPq, Conselho Nacional de Desenvolvimento Científico e Tecnológico support. This work was produced as part of the activity of FAPESP Research, Innovation and Dissemination Center for Neuromathematics (grant #2013/07699-0 S. Paulo Research Foundation).

-
- [1] P. Bak, C. Tang, and K. Wiesenfeld, Phys. Rev. Lett. **59**, 381 (1987).
 - [2] H. J. Jensen, *Self-organized criticality: Emergent Complex Behavior in Physical and Biological Systems* (Cambridge Univ. Press, Cambridge, UK, 1998).
 - [3] R. Dickman, A. Vespignani, and S. Zapperi, Phys. Rev. E **57**, 5095 (1998).
 - [4] R. Dickman, M. A. Muñoz, A. Vespignani, and S. Zapperi, Braz. J. Phys. **30**, 27 (2000).

- [5] J. A. Bonachela and M. A. Muñoz, *J. Stat. Mech.* **2009**, P09009 (2009).
- [6] V. Buendia, S. di Santo, J. A. Bonachela, and M. A. Muñoz, *Frontiers in Physics* **8**, 333 (2020).
- [7] J. M. Beggs and D. Plenz, *J. Neurosci.* **23**, 11167 (2003).
- [8] J. M. Beggs, *Philos. Trans. R. Soc. A* **366**, 329 (2008).
- [9] D. R. Chialvo, *Nature Phys.* **6** (2010).
- [10] M. A. Muñoz, *Rev. Mod. Phys.* **90** (2018).
- [11] T. T. A. Carvalho, A. J. Fontenele, M. Girardi-Schappo, T. Feliciano, L. A. A. Aguiar, T. P. L. Silva, N. A. P. de Vasconcelos, P. V. Carelli, and M. Copelli, *Frontiers in Neural Circuits* **14**, 83 (2021).
- [12] A. Levina, J. M. Herrmann, and T. Geisel, *Nature Phys.* **3**, 857 (2007).
- [13] J. A. Bonachela, S. de Franciscis, J. J. Torres, and M. A. Muñoz, *J. Stat. Mech.* **2010**, P02015 (2010).
- [14] R. Zeraati, V. Priesemann, and A. Levina, *Frontiers in Physics* **9**, 1 (2021), arXiv:2010.07888.
- [15] L. Brochini, A. A. Costa, M. Abadi, A. C. Roque, J. Stolfi, and O. Kinouchi, *Sci. Rep.* **6** (2016).
- [16] A. A. Costa, L. Brochini, and O. Kinouchi, *Entropy* **19**, 399 (2017).
- [17] J. G. F. Campos, A. A. Costa, M. Copelli, and O. Kinouchi, *Phys. Rev. E* **95**, 042303 (2017).
- [18] O. Kinouchi, L. Brochini, A. A. Costa, C. J. G. F, and M. Copelli, *Sci. Rep.* **9**, 3874 (2019).
- [19] M. Girardi-Schappo, B. L, A. A. Costa, T. T. A. Carvalho, and O. Kinouchi, *Phys. Rev. Res.* **2**, 012042 (2020).
- [20] O. Kinouchi, R. Pazinni, and M. Copelli, *Front. Phys.* **8** (2020), 10.3389/fphy.2020.583213.
- [21] A. de Candia, A. Sarracino, I. Apicella, and L. de Arcangelis, *PLOS Computational Biology* **17**, e1008884 (2021).
- [22] W. Gerstner and J. L. van Hemmen, *Netw. Comput. Neural Syst.* **3** (1992).
- [23] A. Galves and E. Löcherbach, *J. Stat. Phys.* **151** (2013).
- [24] D. B. Larremore, W. L. Shew, E. Ott, F. Sorrentino, and J. G. Restrepo, *Phys. Rev. Lett.* **112**, 138103 (2014).
- [25] J. Zierenberg, J. Wilting, V. Priesemann, and A. Levina, *Phys. Rev. Res.* **2**, 013115 (2020).
- [26] M. Girardi-Schappo, E. F. Galera, T. T. A. Carvalho, L. Brochini, N. L. Kamiji, A. C. Roque, and O. Kinouchi, *bioRxiv* (2021), 10.1101/2020.12.17.423201.

- [27] J. M. Beggs and D. Plenz, *J. Neurosci.* **24**, 5216 (2004).
- [28] N. Spruston, Y. Schiller, G. Stuart, and B. Sakmann, *Science* **268**, 297 (1995).
- [29] L. L. Gollo, O. Kinouchi, and M. Copelli, *PLoS Comput. Biol.* **5**, e1000402 (2009).
- [30] A. C. Kreitzer and W. G. Regehr, *Current opinion in neurobiology* **12**, 324 (2002).
- [31] T. Ohno-Shosaku and M. Kano, *Current opinion in neurobiology* **29**, 1 (2014).
- [32] G. Pruessner, *Contemporary Physics*, Vol. 54 (Cambridge University Press, Cambridge, 2012) pp. 175–175.
- [33] V. Priesemann, *BMC Neuroscience* **16**, O19 (2015).
- [34] J. Touboul and A. Destexhe, *Physical Review E* **95**, 1 (2017), arXiv:1503.08033.
- [35] Z. Ma, G. G. Turrigiano, R. Wessel, and K. B. Hengen, *Neuron* **104**, 655 (2019).
- [36] V. Hernandez-Urbina and J. M. Herrmann, *Front Phys* **4**, 54 (2017).
- [37] T. Petermann, T. C. Thiagarajan, M. A. Lebedev, M. A. L. Nicolelis, D. R. Chialvo, and D. Plenz, *Proceedings of the National Academy of Sciences* **106**, 15921 (2009).
- [38] G. Hahn, T. Petermann, M. N. Havenith, S. Yu, W. Singer, D. Plenz, and D. Nikolić, *Journal of Neurophysiology* **104**, 3312 (2010).
- [39] O. Kinouchi and M. Copelli, *Nature Phys.* **2**, 348–351 (2006).